



High-pressure structural behaviour of $\text{Cu}_{0.5}\text{Fe}_{0.5}\text{Cr}_2\text{S}_4$: An experimental and theoretical study



A. Waśkowska^a, L. Gerward^{b,*}, J. Staun Olsen^c, A. Svane^d, G. Vaitheeswaran^e, V. Kanchana^f

^aInstitute of Low Temperature and Structure Research, Polish Academy of Sciences, Wrocław, Poland

^bDepartment of Physics, Technical University of Denmark, Lyngby, Denmark

^cNiels Bohr Institute, Oersted Laboratory, University of Copenhagen, Copenhagen, Denmark

^dDepartment of Physics and Astronomy, Aarhus University, Aarhus, Denmark

^eAdvanced Centre of Research in High Energy Materials, University of Hyderabad, Prof. C. R. Rao Road, Gachbowli, Hyderabad 500 046, Andhra Pradesh, India

^fDepartment of Physics, Indian Institute of Technology Hyderabad, Ordnance Factory Estate, Yeddumailaram 502 205, Andhra Pradesh, India

ARTICLE INFO

Article history:

Received 8 April 2013

Received in revised form 16 May 2013

Accepted 17 May 2013

Available online 24 May 2013

Keywords:

High-pressure X-ray diffraction

Synchrotron radiation

Density functional theory

Bulk modulus

Phase transition

Jahn–Teller effect

ABSTRACT

The structural behaviour of $\text{Cu}_{0.5}\text{Fe}_{0.5}\text{Cr}_2\text{S}_4$ has been studied experimentally and theoretically at pressures up to 44 GPa. The experiments are supported by density functional calculations using the full-potential linear muffin-tin orbital method for investigating ground state properties and high-pressure behaviour. We report here the first experimental and theoretical determinations of the bulk modulus: $B_0 = 106(2)$ GPa and $B'_0 = 4.0$ (experimental), and $B_0 = 96$ GPa and $B'_0 = 3.9$ (calculated). Moreover, a pressure-induced structural and electronic phase transformation occurs at 14.5 GPa accompanied by a volume collapse of about 6%. Tentatively, the high-pressure phase is assigned the defect NiAs structure of Cr_3S_4 type with space group $I2/m$ (12). The mechanism of the phase transition is explained by a Jahn–Teller type distortion, associated with geometrical frustration and magnetic spin changes.

© 2013 Elsevier B.V. All rights reserved.

1. Introduction

The thiospinel $\text{Cu}_{0.5}\text{Fe}_{0.5}\text{Cr}_2\text{S}_4$ exhibits colossal magnetoresistance (CMR) near the Curie temperature $T_c = 345$ K [1,2]. This is interesting because of potential technological applications and remarkable physical properties. The crystal structure of $\text{Cu}_{0.5}\text{Fe}_{0.5}\text{Cr}_2\text{S}_4$ consists of a cubic close packed arrangement of S^{2-} ions with Fe^{3+} and Cu^+ ordered in tetrahedrally coordinated A-sites, and Cr^{3+} occupying octahedral B-sites. At ambient temperature, the spins of the Fe^{3+} and Cr^{3+} ions are aligned antiferromagnetically [3,4]. A recent study of the system $\text{Cu}_x\text{Fe}_{1-x}\text{Cr}_2\text{S}_4$ has shown that the charge state of Fe is Fe^{2+} (ferrous) for $x = 0.1$, and Fe^{3+} (ferric) for $x = 0.5$, whereas a mixed charge state $\text{Fe}^{2+}/\text{Fe}^{3+}$ is found for $0.2 \leq x \leq 0.4$ [5]. This result is interesting, since Fe^{2+} with $3d^6$ electrons is a Jahn–Teller active ion.

The magnetic structure at 10 K, determined by neutron diffraction, does not show any crystallographic distortion. The cubic structure is preserved and all magnetic reflections overlap the nuclear ones [4,5]. Structure refinement shows that the ferrimagnetic character of the magnetic couplings results from antiparallel alignment of the ferromagnetically ordered magnetic moments in the Fe and Cr sublattices. A remarkable feature of the low-

temperature structure is the localized magnetic moment of $3.1 \mu_B$ for Fe, which is less than $5.0 \mu_B$ for purely ionic Fe^{3+} with $3d^5$ electrons. The difference has been explained by a strong hybridization of the Fe $3d$ and S $3p$ bands. Together with the elongation of the Fe–S bond, which had been expected to contract on cooling like the Cu–S bond, these effects are indicating mixed $\text{Fe}^{3+}/\text{Fe}^{2+}$ and $\text{Cu}^+/\text{Cu}^{2+}$ ionic states.

Several authors have studied the structural, magnetic and electronic properties of $\text{Cu}_{0.5}\text{Fe}_{0.5}\text{Cr}_2\text{S}_4$ at ambient pressure, room temperature and low or high temperature [2–11]. However, to our best knowledge, no studies of $\text{Cu}_{0.5}\text{Fe}_{0.5}\text{Cr}_2\text{S}_4$ under high pressure have been carried out until now. High pressure should be interesting, since it would enhance the crystal field and possibly induce structural and electronic changes in the material. This prompted us to perform an experimental and theoretical investigation of the high-pressure structural behaviour of $\text{Cu}_{0.5}\text{Fe}_{0.5}\text{Cr}_2\text{S}_4$ using synchrotron X-ray diffraction and density functional calculations. As the results will show, there is indeed a pressure-induced structural and electronic phase transition, reducing symmetry to lower than cubic. In the discussion we are focusing on a Jahn–Teller-type distortion associated with geometrical frustration and electron spin distribution in the transition metals concerned.

* Corresponding author. Tel.: +45 45253146.

E-mail address: gerward@fysik.dtu.dk (L. Gerward).

2. Experimental and theoretical procedures

High-pressure X-ray diffraction powder spectra were recorded at the synchrotron radiation facility HASYLAB-DESY in Hamburg, Germany, using the white-beam method and a diamond-anvil cell of Syassen–Holzapfel type. Silicone oil was used as the pressure-transmitting medium, and the pressure was determined by the ruby luminescence method [12]. The Birch–Murnaghan equation of state [13] was fitted to the experimental pressure–volume data.

The electronic structure of $\text{Cu}_{0.5}\text{Fe}_{0.5}\text{Cr}_2\text{S}_4$ was calculated with the linear muffin-tin orbital (LMTO) method [14] in the full-potential (FP) implementation of Methfessel [15] and Methfessel et al. [16]. The effects of exchange and correlation were treated with the local spin density approximation (LSDA), as parameterized by Vosko et al. [17], or with the generalized gradient approximation (GGA), as parameterized by Perdew et al. [18]. In the FP-LMTO method, the crystal volume is divided into two regions: non-overlapping muffin-tin spheres around each atom, and the remaining interstitial space between the atoms [15]. A triple κ *spdf* LMTO basis is used to describe the valence electrons, i.e. Hankel-functions characterized by decay constants κ are smoothly augmented inside the atomic spheres with numerical radial functions. The basis set was further augmented with orbitals centred on interstitial positions. The charge sampling was performed with the tetrahedron method [19,20] with a $12 \times 12 \times 12$ ($8 \times 8 \times 8$) mesh of the Brillouin zone for the cubic (monoclinic) phase, corresponding to 182 (128) irreducible k -points, respectively.

3. Results and discussion

3.1. Lattice parameter and interplanar spacing

The crystal structure of the cubic thiospinel $\text{Cu}_{0.5}\text{Fe}_{0.5}\text{Cr}_2\text{S}_4$ is of the MgAl_2O_4 type, and there are eight formula units per unit cell [21]. In the present work, the relative atomic coordinates have been taken from Riedel et al. [22]. In X-ray diffraction studies, the space group is generally given as $Fd\bar{3}m$ (227) as for normal spinels, i.e. assuming random distribution of Cu and Fe at A-sites. However, weak superstructure reflections, observed by neutron diffraction, show that symmetry is reduced by positional order of Cu and Fe ions occupying different tetrahedral sites (4a and 4d) in the true space group $F43m$ (216) [3,4,23,24].

Fig. 1 shows a diffraction spectrum of cubic $\text{Cu}_{0.5}\text{Fe}_{0.5}\text{Cr}_2\text{S}_4$. The lattice parameter at ambient conditions, determined as the mean value of several runs, is $a_0 = 9.906(2)$ Å. The theoretical value, calculated at $T = 0$ K in the GGA approach, is $a_0 = 9.898$ Å. These results together with other published data are shown in Table 1. Our experimental and theoretical results are in particularly good agreement with the experimental values of Palmer and Greaves [3,4] at room temperature, and at 10 K.

Fig. 2 shows the observed interplanar spacing d as a function of pressure. Miller indices of the cubic reflections are shown to the left. There is clearly a structural phase transformation with

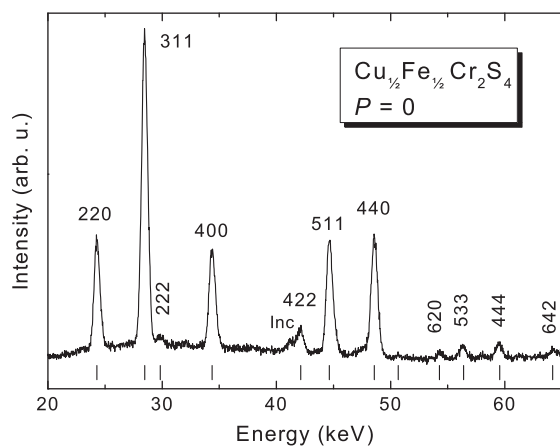


Fig. 1. X-ray diffraction spectrum of $\text{Cu}_{0.5}\text{Fe}_{0.5}\text{Cr}_2\text{S}_4$ at ambient conditions. The Bragg angle is $\theta = 4.2^\circ$. The row of bars below the spectrum indicates the calculated positions of the Bragg peaks of the cubic spinel structure. Inc = inconel peak.

Table 1

The lattice parameter a_0 of cubic $\text{Cu}_{0.5}\text{Fe}_{0.5}\text{Cr}_2\text{S}_4$ at ambient pressure. The values are for room temperature where not otherwise stated.

a_0 (Å)	Reference
9.904	Riedel et al. [22]
9.901	Zaritskii et al. [23]
9.922	Ok et al. [25]
9.907	Palmer and Greaves [3]
9.898	Palmer and Greaves, $T = 10$ K [4]
9.900	Sadykov et al. [24]
9.880	Sadykov et al., $T = 2$ K [24]
9.923 ^a	Fritsch et al. [2]
9.866	Son et al. [5]
9.906	Present work, expt.
9.898	Present work, GGA calc.

^a Read from graph.

a transition pressure P_{tr} of about 14.5 GPa, where new diffraction lines are appearing. The crystal structure of the high-pressure phase will be discussed in Section 3.3.

3.2. Bulk modulus and the equation of state for the cubic phase

Fig. 3 shows the volume per formula unit as a function of pressure. A Birch–Murnaghan fit for $P < 7$ GPa gives the experimental bulk modulus $B_0 = 106(2)$ GPa and $B'_0 = 4.0$. These values are in reasonably good agreement with the calculated values $B_0 = 96$ GPa and $B'_0 = 3.9$ (Table 2). To our best knowledge, there are no values in the literature, with which the present results can be compared. Fig. 3 also shows that the experimental pressure–volume data for the cubic phase slightly deviates from the extrapolated Birch–Murnaghan equation above 7 GPa, possibly a precursor of the phase transition at 14.5 GPa.

3.3. Crystal structure of the high-pressure phase

Compounds of the type AB_2X_4 where A and B are transition metals and X a chalcogen, usually have the spinel structure or a defect NiAs structure with ordered vacancies [26]. The latter structure, which is of the Cr_3S_4 type, is monoclinic with a bimolecular unit cell [27]. The space group is $I2/m$ (12). In the spinel structure, one-third of the cations are in tetrahedral sites and two-thirds in octahedral sites. In the defect NiAs structure, on the other hand, all cations are in octahedral sites, leading to higher coordination

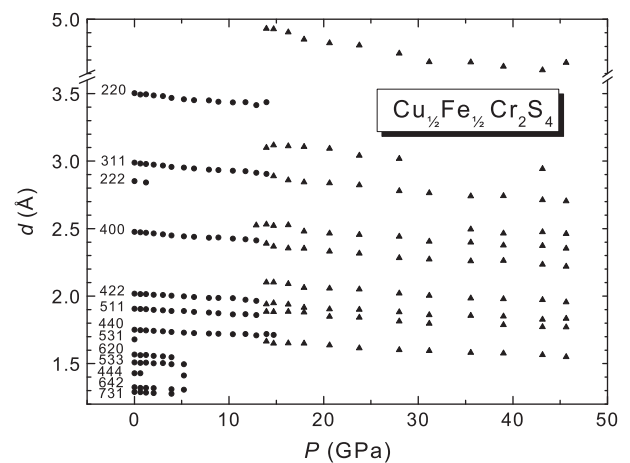


Fig. 2. Observed d spacing as a function of pressure. Circles denote data points for the cubic phase, and the corresponding Miller indices are given at the left-hand side. Triangles denote data points for the high-pressure phase.

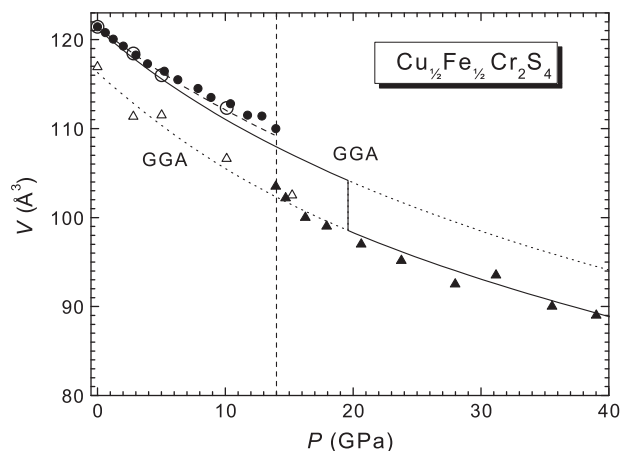


Fig. 3. Compression curves of $\text{Cu}_{0.5}\text{Fe}_{0.5}\text{Cr}_2\text{S}_4$. V is the volume per formula unit, and P is the pressure. Circles denote experimental data points for the cubic phase, and triangles the monoclinic phase. Filled symbols denote compression, and open symbols decompression. The dashed curve is the fit of the Birch–Murnaghan equation for $P < 7$ GPa and extrapolated up to the experimental transition pressure 14.5 GPa (vertical dashed line). The full and dotted curves are the results of the GGA calculation for the cubic and monoclinic phases. The theoretical transition occurs at 19.6 GPa.

and density, which is typical for a high-pressure phase. For sulphides ($X = \text{S}$), both structures occur, indicating a small energy difference between the two forms. For example, NiCr_2S_4 has the monoclinic structure already at ambient conditions [28,29]. We conclude that the defect NiAs structure of Cr_3S_4 type is a highly probable candidate for the high-pressure phase of $\text{Cu}_{0.5}\text{Fe}_{0.5}\text{Cr}_2\text{S}_4$. It may be mentioned that a similar monoclinic phase has been observed for the related compound $\text{Co}_{0.65}\text{Ni}_{0.35}\text{Cr}_2\text{S}_4$ [30].

Fig. 4 shows the X-ray diffraction spectrum of the high-pressure phase at 28 GPa. The energy dispersive method, used in the present work, does not resolve the individual Bragg reflections of the low-symmetry high-pressure phase, and the observed spectrum therefore consists of a number of broad sum peaks. However, the calculated peak positions of the possible monoclinic defect NiAs structure (shown as a row of vertical bars at the bottom of Fig. 4) clearly indicate that the observed sum peaks agree well with the main groups of calculated individual reflections. We therefore feel confident that the high-pressure phase of $\text{Cu}_{0.5}\text{Fe}_{0.5}\text{Cr}_2\text{S}_4$ is indeed the monoclinic defect NiAs structure of Cr_3S_4 type.

A full structural analysis of the monoclinic phase has not been possible in the present work, since the individual Bragg reflections are not resolved. However, we have performed a tentative analysis of the unit-cell volume as a function of pressure, using the strongest peaks of the monoclinic phase. The result is shown in Fig. 3. It is seen that the experimental pressure–volume data points are reasonably close to the theoretical curves, albeit with some scatter. The experimental volume change at the transition pressure 14.5 GPa is $\Delta V/V = -6.0(3)\%$, which agrees well with the calculated value -5.7% (Table 2). Upon decompression, the sample reverts to the cubic structure. The back-transition is sluggish, however, and there are traces of the monoclinic phase even at ambient pressure.

Table 2

Values of the bulk modulus B_0 and its pressure derivative B'_0 for cubic $\text{Cu}_{0.5}\text{Fe}_{0.5}\text{Cr}_2\text{S}_4$. Also included are values of the transition pressure, P_{tr} , and the relative volume change, $\Delta V/V$, at the transition.

B_0 (GPa)	B'_0	P_{tr} (GPa)	$\Delta V/V$ (%)	Reference
106(3)	4.0	14.5(5)	-6.0(3)	Present work, expt.
96	3.9	19.6	-5.7	Present work, GGA calc.

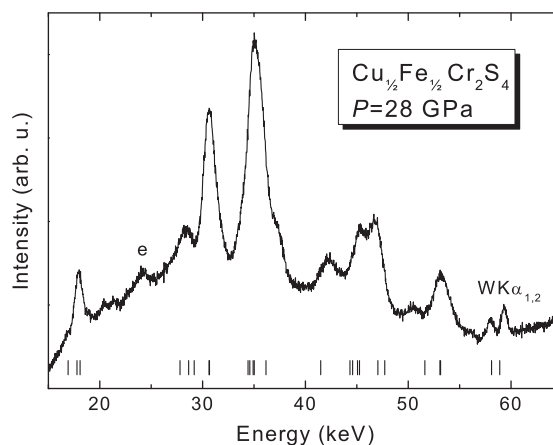


Fig. 4. Diffraction spectrum of $\text{Cu}_{0.5}\text{Fe}_{0.5}\text{Cr}_2\text{S}_4$ at 28 GPa showing broad sum peaks of the high-pressure phase. The Bragg angle is $\theta = 4.2^\circ$; e = escape peak. The row of bars below the spectrum indicates the calculated positions of the individual Bragg peaks of the monoclinic phase.

3.4. Structural and electronic properties of the high-pressure phase

The findings above are supported by calculations using density functional theory with the GGA functional as outlined in Section 2. In these calculations we have used the internal atomic positions as reported for the cubic $\text{Cu}_{0.5}\text{Fe}_{0.5}\text{Cr}_2\text{S}_4$ ($u_0 = 0.383$) at ambient pressure [22], and the structural parameters reported for Cr_3S_4 [27] for the high-pressure monoclinic phase. Andron and Bertaut [28] give almost the same atomic positions for monoclinic NiCr_2S_4 , so these coordinates seem to be rather constant for various compounds with this structure. We have further assumed that the Cu and Fe atoms are occupying the (2a) positions in an ordered fashion. Pressure is varied by uniformly scaling of the lattice parameters, keeping the beta angle and the internal coordinates constant. Fig. 5 shows the calculated total energy as a function of volume for the cubic and monoclinic phases. The common tangent defines the transition point, where the enthalpies of the two phases are equal (at $T = 0$ K). The total-energy curve for the corresponding calculation

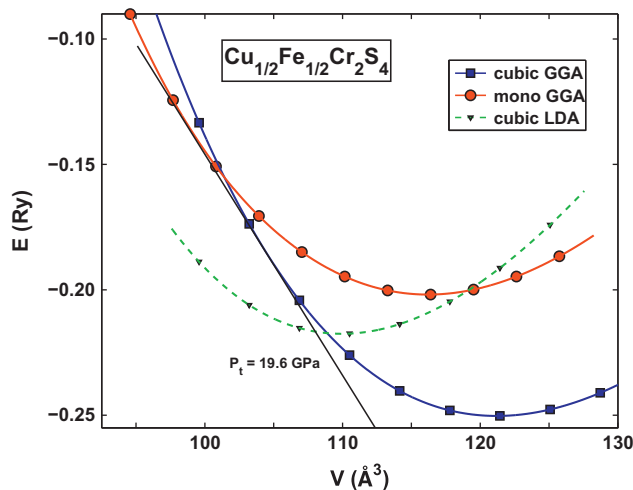


Fig. 5. Total energy (in units of Rydberg per formula unit, and calculated with the GGA total energy functional) of $\text{Cu}_{0.5}\text{Fe}_{0.5}\text{Cr}_2\text{S}_4$ as a function of the volume per formula unit. The cubic and monoclinic structures are considered. The common tangent defines the transition point, where the enthalpies of the two phases are equal. The calculated transition pressure is 19.6 GPa. The dashed (green) curve is the result of an LSDA calculation (not used in the present work). (For interpretation of the references to colour in this figure legend, the reader is referred to the web version of this article).

using the LSDA is included just to show how poorly LSDA is performing for this compound.

The calculated compression curves for the cubic and monoclinic phases are shown in Fig. 3. The theoretical phase transition occurs at 19.6 GPa with a volume collapse of 5.7%. The latter value is in good agreement with experiment. On the other hand, the agreement with the experimental transition pressure of 14.5 GPa is not particularly good. Part of the reason may be that the calculation does not allow for relaxation of the atomic coordinates and the c/a and b/a ratios. Anyway, the calculations confirm that the monoclinic defect NiAs structure is a likely candidate for the high-pressure phase and reproduce the qualitative picture of the experimental observations. The experimental and theoretical results are summarized in Table 2.

The calculated density of electronic states (DOS) is displayed in Fig. 6 for the ambient cubic spinel structure, and in Fig. 7 for the monoclinic phase at 19.6 GPa, corresponding to the theoretical transition pressure. The top panel of the figures shows the DOS summed over spin-component. All three panels of each figure refer to the same spin-polarized calculation. At ambient pressure, the $S p$ bands, which fall in the energy range from -6 eV to 0 eV with respect to the Fermi level, dominate the valence bands. The $Cr d$ states fall in the region around the Fermi level leading to a significant hybridization into the top of the $S p$ bands, and correspondingly significant $Cr d-S p$ antibonding states occur above the Fermi level. A pseudogap forms at the Fermi level separating the bonding and antibonding $S-Cr$ states. Hence the ideal ionic picture of the S^{2-} ions is greatly distorted. The total numbers of valence electrons inside the atomic spheres are listed in Table 3. These charges must be taken with a grain of salt, since they depend on

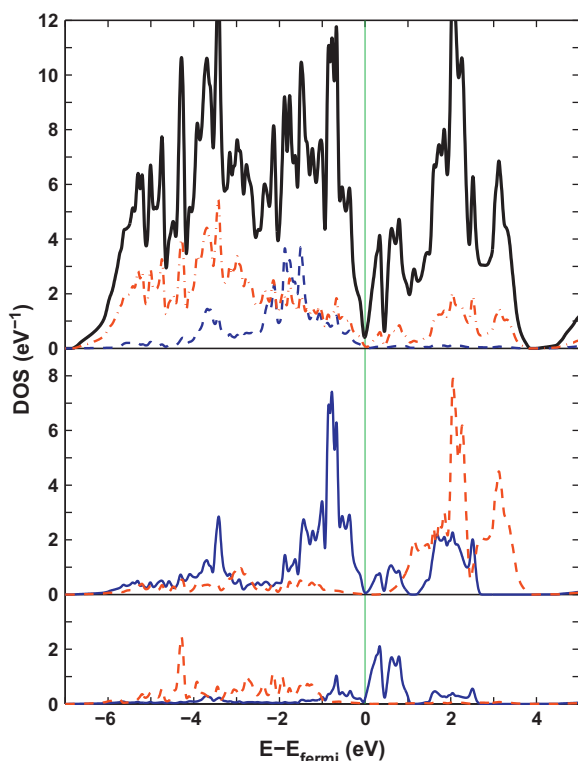


Fig. 6. Density of states for cubic $Cu_{0.5}Fe_{0.5}Cr_2S_4$ at ambient pressure. Top panel: Total density of states (full line) and Cu (dashed) and S (dashed-dotted) partial densities of states (summed over spins); Middle panel: Cr partial density of states projected onto majority (full) and minority (dashed) spin components; Bottom panel: Fe partial and spin decomposed density of states. Units are per eV and per $Cu_{0.5}Fe_{0.5}Cr_2S_4$ formula unit. The thin vertical (green) line marks the Fermi level. (For interpretation of the references to colour in this figure legend, the reader is referred to the web version of this article).

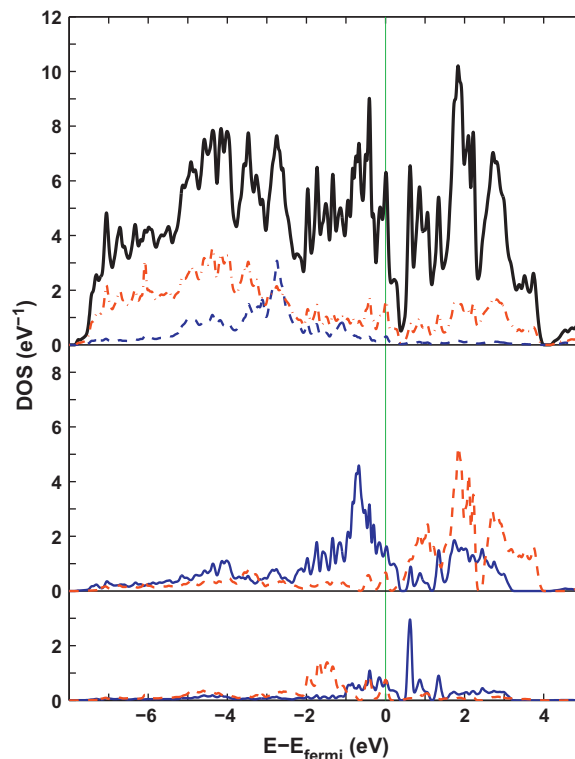


Fig. 7. As Fig. 6 but for the monoclinic phase at a calculated pressure of 19.6 GPa.

Table 3

Calculated numbers n of elementary charges and spin magnetic moments μ in cubic $Cu_{0.5}Fe_{0.5}Cr_2S_4$ at ambient pressure, and in the monoclinic phase at the calculated transition pressure 19.6 GPa. The charges are integrated valence charges within the atomic spheres and in the interstitial region, respectively. The charges are averaged over non-equivalent elements. Only the Cr and Fe moments as well as the total moment per formula unit are given. The atomic radii used in the calculations for the cubic phase are $r(Fe) = 1.138$ Å, $r(Cu) = 1.095$ Å, $r(Cr) = 1.212$ Å and $r(S) = 1.164$ Å; and for the monoclinic phase $r(Fe) = 1.154$ Å, $r(Cu) = 1.148$ Å, $r(Cr) = 1.138$ Å and $r(S) = 1.180$ Å.

	Cubic	Monoclinic
$n(Cr)$	4.48	4.29
$n(Fe)$	6.35	6.57
$n(Cu)$	9.53	9.80
$n(S)$	4.60	4.78
n_{int}	10.20	10.11
$\mu(Cr)$	2.67	2.25
$\mu(Fe)$	-3.19	-2.12
μ_{tot}	3.57	3.76

the specific choice of radii for the atomic spheres, and a considerable charge is also found outside the atomic spheres (the interstitial charge n_{int} in Table 3). Our experience is that different (reasonable) sphere choices may lead to integrated charges fluctuating by about 0.1. The actual radii used in the present calculations are given in the caption of Table 3.

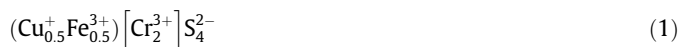
The spin decomposed partial densities of states for Cr and Fe are also shown in Fig. 6 (middle and bottom). It is seen that the Fe and Cr spin charges are oppositely aligned, i.e. $Cu_{0.5}Fe_{0.5}Cr_2S_4$ is ferrimagnetic. The Fe ion is almost fully polarized with the majority component (anti-parallel to the Cr spin direction) hybridizing broadly into the $S p$ valence bands. A significant Fe d occupancy of minority character occurs just below the Fermi level, leaving Fe qualitatively as a d^6 ion. The total numbers of Fe d electrons inside the atomic sphere are 4.48 (majority) and 1.33 (minority),

with a magnetic moment inside the atomic sphere of $-3.19 \mu_B$. In contrast, the Cr moment is $\mu(\text{Cr}) = 2.67 \mu_B$, while the moments forming on Cu and S atoms are negligible. The interstitial region still carries a small magnetization. The total moment of $\text{Cu}_{0.5}\text{Fe}_{0.5}\text{Cr}_2\text{S}_4$ is $\mu_{\text{tot}} = 3.51 \mu_B$.

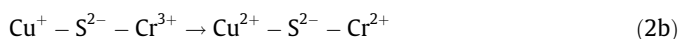
The density of states for the monoclinic phase in Fig. 7 is similar to that of the cubic structure (Fig. 6), however the pseudogap at the Fermi level is now absent, while a different pseudogap occurs about 0.4 eV above the Fermi level. The valence bands are still dominated by S *p* states, now about 1 eV wider, which is a natural consequence of compression. The Fe and Cr magnetic moments have decreased, but because of the ferrimagnetic coupling and the Fe moment decreasing most, it so happens that the total moment in the unit cell is larger in the monoclinic phase at high pressures than in the cubic phase at ambient pressure.

The phase transition is associated with macroscopic strains, which increase gradually with increasing pressure. Strains originate from inherent geometrical frustration and magnetic spin frustration in the A-sites, accommodating Fe and Cu ions with different chemical and magnetic properties. The geometrical frustration arises from FeS_4 and CuS_4 tetrahedra, containing diamagnetic Cu^+ and ferric Fe^{3+} ions with very different radius (0.60 Å and 0.49 Å, respectively) [31]. In terms of the ligand field theory such a system is energetically unstable, and the strain-induced instability can be released by a Jahn–Teller distortion, resulting in symmetry lower than cubic.

At ambient pressure, $\text{Cu}_{0.5}\text{Fe}_{0.5}\text{Cr}_2\text{S}_4$ has the following valences:



where () denotes tetrahedral A-sites, and [] octahedral B-sites. This compound does not contain any Jahn–Teller active cations. However, long-range magnetic order enables various anion-mediated electron exchange interactions at the B-sites, and between the A and B-sublattices, below the critical temperature T_c . In our case, similar exchange interactions may occur at high pressure. The first-order character of the phase transition indicates a strong interaction between the two sublattices. The Zener-type double exchange interactions between A- and B-sites:



will create a corresponding number of Cr^{4+} and Cr^{2+} ions in octahedral B-sites. Thus, the chemical formula can now be written:



It may be expected that ferromagnetic Kramers–Anderson super exchange will occur at the octahedral sites in the same way as in other chromium-based spinels, since $\text{Cr}^{4+}(t_{2g}^3 e^1)$ donating one electron to $\text{Cr}^{2+}(t_{2g}^2)$ are connected at 90° to the bridging S^{2-} , cf. [32]. The alternating $\text{Cr}^{2+}-\text{S}^{2-}-\text{Cr}^{4+}$ coupling leads to a spin configuration of Cr^{3+} with half-filled t_{2g}^3 orbitals.

The above charge transfers result in an oxidation of copper and a reduction of the ferric ions. The resulting Cu^{2+} , with electronic spin distribution $e^4 t_2^1$, has one unpaired electron spin in t_2 triplet state and is therefore Jahn–Teller active, causing a $c/a < 1$ contraction of the coordinating polyhedron. Moreover, the increased Cu valence makes the Cu–S bonds more covalent, and this may influence the lattice–electron coupling.

In the low-temperature structure at 10 K, it is found that the Fe–S bond distance has expanded while the Cu–S bond, as expected, has contracted as compared with the structure at room temperature [3,4]. Since the ionic radii of Fe^{3+} and Fe^{2+} are 0.49 and 0.63 Å, respectively, this behaviour suggests the valence state of some of the Fe-ions are reduced to Fe^{2+} , though no anomalies in

the temperature dependences of the unit cell were observed. Moreover, the difference between the experimental value of the Fe magnetic moment ($3.1 \mu_B$) and that of an ideal Fe^{3+} ion ($5.0 \mu_B$) indicates a reduction of Fe^{3+} to Fe^{2+} and in addition a change of the electron spin distribution in Fe^{2+} . This is also consistent with the present GGA calculations (cf. Table 3).

It is known that the ionic spin state depends on the energy of the crystal field, and the latter may be changed by temperature, pressure or a magnetic field [33–35]. High-pressure enhances the ligand field strength Δ for a number of compounds such as perovskites [36,37], the 3d transition metal chalcogenides [38–41], and the quarternary oxides [42–44]. This may induce a change in the electronic spin distribution of the cation orbitals. The effect, referred to as spin crossover or high-spin (HS) to low-spin (LS) transition, is typically observed for cations in the octahedral ligand field [45,46]. There is scarce information on possible spin crossover in a tetrahedral field.

The energy of the tetrahedral ligand field splits the five 3d orbitals into a lower-energy doublet (*e*) and a higher-energy triplet (*t₂*). The splitting energy of the tetrahedral field Δ_t is only 4/9 of that of the octahedral field Δ_0 at ambient conditions. Therefore, Δ_t is not large enough to pair electrons in the *e* orbitals before filling the higher energy *t₂* states. Thus, in a weak field, the ground state of the A-site cations is usually HS, since the electron pairing energy is larger than the energy Δ_t required for exciting the electrons into the higher-energy orbitals. At sufficiently high pressure, the magnitude of the orbital splitting Δ_t may exceed the spin-pairing energy, thus causing a HS-to-LS transition.

At ambient pressure the HS configuration of the valence electrons of Fe^{2+} , $e^3 t_2^3 (e^3 \uparrow \downarrow \uparrow t_2^3 \uparrow \uparrow \uparrow)$, has four unpaired electron spins. It is reasonable to assume that the density of the compound increases in the pressure-induced crystal field, thereby changing the spin configuration to the LS state $e^4 t_2^2 (e^4 \uparrow \downarrow \uparrow \downarrow t_2^2 \uparrow \uparrow)$ with only two unpaired spins. The HS–LS transition leads to a decrease in the magnetic moment of Fe^{2+} consistent with the observation of a magnetic moment lower than expected and explaining the anomalous Fe–S bond behaviour [3,4]. The impact of the HS–LS transition is expected to be more pronounced at high pressure than at low temperature, because of the enhancement of the crystal field at high pressure.

In summary, we consider the transition at 14.5 GPa as being driven by two coupled effects: (1) the Jahn–Teller activity of Cu^{2+} , relieving the structure from the geometric frustration; (2) electronic spin pairing of Fe^{2+} , leading to a state of spin equilibrium in the pressure-enhanced crystal field.

4. Conclusions

We are here reporting the first experimental and theoretical determinations of the bulk modulus of cubic spinel phase of $\text{Cu}_{0.5}\text{Fe}_{0.5}\text{Cr}_2\text{S}_4$. Moreover, a pressure-induced structural phase transformation has been observed with a transition pressure of 14.5 GPa and a volume collapse of about 6%. Tentatively, the high-pressure phase is assigned the defect NiAs structure of Cr_3S_4 type. The experimental results are supported and confirmed by theoretical density functional calculations. We suggest that long-range magnetic interactions of super exchange and double exchange type are responsible for valence and spin changes. The resulting strong Jahn–Teller activity of Cu^{2+} , together with the high-spin to low-spin transition of Fe^{2+} , would then be the main factors causing the observed structural phase transformation.

Acknowledgements

We thank HASYLAB-DESY for permission to use the synchrotron radiation facility. A.W., L.G., J.S.O. and A.S. gratefully acknowledge

financial support from the Danish Natural Sciences Research Council, the former three through DANSCATT.

References

- [1] A.P. Ramirez, R.J. Cava, J. Krajewski, *Nature* 386 (1997) 156.
- [2] V. Fritsch, J. Deisenhofer, R. Fichtl, J. Hemberger, H.-A. Krug von Nidda, M. Müksch, M. Nicklas, D. Samusi, J.D. Thompson, R. Tidecks, V. Tsurkan, A. Loidl, *Phys. Rev. B* 67 (2003) 144419.
- [3] H.M. Palmer, C. Greaves, *J. Mater. Chem.* 9 (1999) 637.
- [4] H.M. Palmer, C. Greaves, *Physica B* 276–278 (2000) 568.
- [5] B.S. Son, S.J. Kim, I.-B. Shim, B.W. Lee, C.S. Kim, *Hyperfine Interact.* 169 (2006) 1285.
- [6] Z. Klencsár, E. Kuzmann, Z. Homonnay, Z. Németh, I. Virág, M. Kühberger, G. Gritzner, A. Vértés, *Physica B* 358 (2005) 93.
- [7] A. Deb, N. Hiraoka, M. Itou, Y. Sakurai, *Phys. Rev. B* 66 (2002) 100407(R).
- [8] A. Deb, M. Mizumaki, T. Muro, Y. Sakurai, V. Tsurkan, *Phys. Rev. B* 68 (2003) 014427.
- [9] J.-S. Kang, S.J. Kim, C.S. Kim, C.G. Olson, B.I. Min, *Phys. Rev. B* 63 (2001) 14412.
- [10] V. Tsurkan, S. Plogmann, M. Demeter, D. Hartmann, M. Neumann, *Eur. Phys. J. B* 15 (2000) 401.
- [11] E.Z. Kurmaev, A.V. Postnikov, H.M. Palmers, C. Greaves, S. Bartkowski, V. Tsurkan, M. Demeter, D. Hartmann, M. Neumann, D.A. Zatsepin, V.R. Galakhov, S.N. Shamin, V. Trofimova, *J. Phys.: Condens. Matter* 12 (2000) 5411.
- [12] H.K. Mao, J. Xu, P.M. Bell, *J. Geophys. Res.* 91 (1986) 4673.
- [13] F.J. Birch, *J. Geophys. Res.* 83 (1978) 1257.
- [14] O.K. Andersen, *Phys. Rev. B* 12 (1975) 3060.
- [15] M. Methfessel, *Phys. Rev. B* 38 (1988) 1537.
- [16] M. Methfessel, C.O. Rodríguez, O.K. Andersen, *Phys. Rev. B* 40 (1989) 2009.
- [17] S.H. Vosko, L. Wilk, M. Nusair, *Can. J. Phys.* 58 (1980) 1200.
- [18] J.P. Perdew, K. Burke, M. Ernzerhof, *Phys. Rev. Lett.* 77 (1996) 3865.
- [19] O. Jepsen, O.K. Andersen, *Solid State Commun.* 9 (1971) 1763.
- [20] G. Lehmann, M. Taut, *Phys. Status Solidi B* 54 (1972) 469.
- [21] R.W.G. Wyckoff, *Crystal Structures*, Interscience, second ed., vol. 3, J. Wiley & Sons, New York, 1965, p. 75.
- [22] E. Riedel, R. Karl, R. Rackwitz, *J. Solid State Chem.* 40 (1981) 255.
- [23] V.N. Zaritskii, R.A. Sadykov, Y.I. Kostyuk, R.A. Sizov, T.G. Aminov, R.K. Gubaidullin, S.R. Safin, *Soviet Phys. Solid State* 28 (1986) 1854.
- [24] R.A. Sadykov, V.N. Zaritskii, J. Mesot, F. Fauth, *Crystallogr. Rep.* 46 (2001) 21.
- [25] H.N. Ok, K.S. Baek, H.S. Lee, C.S. Kim, *Phys. Rev. B* 41 (1990) 62.
- [26] R.J. Bouchard, *Mater. Res. Bull.* 2 (1967) 459.
- [27] R.W.G. Wyckoff, *Crystal Structures*, Interscience, second ed., vol. 2, J. Wiley & Sons, New York, 1964, p. 150.
- [28] B. Andron, E.F. Bertaut, *Le J. de Physique (Paris)* 27 (1966) 619.
- [29] A.V. Powell, D.C. Colgan, C. Ritter, *J. Solid State Chem.* 134 (1997) 110.
- [30] P. Vaqueiro, A.V. Powell, S. Hull, D.A. Keen, *Phys. Rev. B* 63 (2001) 064106.
- [31] R.D. Shannon, *Acta Crystogr. A* 32 (1976) 751.
- [32] P.K. Baltzer, P.J. Wojtowicz, M. Robbins, E. Lopatin, *Phys. Rev.* 151 (1966) 367.
- [33] J.D. Dunitz, L.E. Orgel, *J. Phys. Chem. Solids* 3 (1957) 20.
- [34] F. Wells, *Structural Inorganic Chemistry*, fifth ed., Clarendon, Oxford, 1984, pp 86–92.
- [35] L.E. Orgel, *Introduction to Transition-Metal Chemistry: Ligand Field Theory*, Methuen, London, 1960.
- [36] M. Takano, S. Nasu, T. Abe, K. Yamamoto, S. Endo, Y. Takeda, J.B. Goodenough, *Phys. Rev. Lett.* 67 (1991) 3267.
- [37] C. Zobel, M. Kriener, D. Bruns, J. Baier, M. Grüniger, T. Lorenz, P. Reutler, A. Revcolevschi, *Phys. Rev. B* 66 (2002) 020402(R).
- [38] J.-P. Rueff, C.-C. Kao, V.V. Struzhkin, J. Badro, R.J. Hemley, H.-K. Mao, *Phys. Rev. Lett.* 82 (1999) 3284.
- [39] S.S. Naghavi, S. Chadov, C. Felser, *J. Phys.: Condens. Matter* 23 (2011) 205601.
- [40] J.-F. Lin, V.V. Struzhkin, S.D. Jacobsen, M.Y. Hu, P. Chow, J. Kung, H. Liu, H.-K. Mao, R.J. Hemley, *Nature* 436 (2005) 377.
- [41] M. Womes, C. Reibel, A. Mari, D. Zitoun, *J. Solid State Chem.* 184 (2011) 753.
- [42] B.J. Kennedy, Q. Zhou, *J. Solid State Chem.* 181 (2008) 2227.
- [43] T. Vogt, P.M. Woodward, P. Karen, B.A. Hunter, P. Henning, A.R. Moodenbaugh, *Phys. Rev. Lett.* 84 (2000) 2969.
- [44] S.V. Streltsov, N.A. Skorikov, *Phys. Rev. B* 83 (2011) 214407.
- [45] G.G. Levchenko, V. Ksenofontov, A.V. Stupakov, H. Spiering, Y. Garcia, P. Gütllich, *Chem. Phys.* 277 (2002) 125.
- [46] P. Gütllich, V. Ksenofontov, A.B. Gaspar, *Coord. Chem. Rev.* 249 (2005) 1811.